

Soil moisture modelling with ERA5-Land retrievals, topographic indices and in-situ measurements and its use for predicting ruts

Marian Schönauer¹, Anneli M. Ågren², Klaus Katzensteiner³, Florian Hartsch¹, Paul Arp⁴, Simon Drollinger⁵, Dirk Jaeger¹

¹Department of Forest Work Science and Engineering, University of Göttingen, Göttingen, Germany

²Department of Forest Ecology and Management, Swedish University of Agricultural Sciences, Umeå, Sweden

³Institute of Forest Ecology, University of Natural Resources and Life Sciences, Vienna, Vienna, Austria

⁴Forestry and Environmental Management, University of New Brunswick, New Brunswick, Canada

⁵Department of Physical Geography, University of Göttingen, Göttingen, Germany

Correspondence to: Marian Schönauer (marian.schoenauer@uni-goettingen.de)

Abstract

Spatiotemporal modelling is an innovative way of predicting soil moisture and has promising applications in supporting sustainable forest operations. One such application is the prediction of rutting, since rutting can cause severe damage to forest soils and ecological functions.

In this work, we used ERA5-Land soil moisture retrievals and several topographic indices to model variations of in-situ soil water content, by means of a random forest model. We then correlated the predicted soil moisture with rut depth from different trials.

Our spatiotemporal modelling approach successfully predicted soil moisture with a Kendall's rank correlation coefficient of 0.62 (R^2 of 64%). The final model included the spatial depth-to-water index, topographic wetness index, stream power index, as well as temporal components such as month and season, and ERA5-Land soil moisture retrievals. These retrievals showed to be the most important predictor in the model, indicating a large temporal variation. The prediction of rut depth was also successful, resulting in a Kendall's correlation coefficient of 0.61.

Our results demonstrate that by using data from several sources, including ERA5-Land retrievals, topographic indices and in-situ soil moisture measurements, we can accurately predict soil moisture and use this information to predict rut depth. This has practical applications in reducing the impact of heavy machinery on forest soils and avoiding wet areas during forest operations.

Keywords: spatiotemporal modelling, forest management, forest engineering, rutting, downscaling, reanalysis

1 Introduction

For decades, forestry research has sought solutions to accurately predict the trafficability of forest soils (Mattila and Tokola, 2019; White et al., 2012; Murphy et al., 2007). In order to further sustainable forest management, efficient protection of forest soils is mandatory (Vega-Nieva et al., 2009; Picchio et al., 2020; Uusitalo et al., 2019). Heavy harvesting and forwarding machines have been frequently associated with severe soil damage, particularly when operating on soils with low bearing capacity (Horn et al., 2007; Allman et al., 2017). Soil compaction is a common consequence of harvesting operations (Ampoorter et al., 2010; Eliasson, 2005; DeArmond et al., 2021) and has been shown to be detrimental to a number of

35 ecological functions, including soil biota (Beylich et al., 2010), hydrological patterns, and nutrient supply, with potential
36 drawbacks on plant growth and site productivity (Curzon et al., 2022). In addition to soil compaction, machine traffic can also
37 result in deep ruts (Horn et al., 2007; Ala-Ilomäki et al., 2021; Poltorak et al., 2018), which affect site hydrology and increase
38 anaerobic conditions at the rut's base, where air-filled porosity is reduced, leading to minimized soil aeration (Hansson et al.,
39 2019).

40 The risk of causing high degrees of soil compaction and rutting is mainly attributed to soil properties such as initial soil bulk
41 density and texture, as well as the current soil water content (Cambi et al., 2015; Crawford et al., 2021). Moist soils show a
42 higher susceptibility to damage since the internal friction is decreased through water embracing soil particles (Hillel, 1998),
43 reducing the soil bearing capacity and the ability for elastic responses to machine-induced impacts (McNabb et al., 2001).

44 To support forestry management and machine operators, accurate cartographic information on soils with low bearing capacity
45 is essential (Jones and Arp, 2017; Sirén et al., 2019; Campbell et al., 2013). However, existing models that rely on detailed
46 soil maps to retrieve soil mechanical parameters (e.g. Grull, 2011; Heubaum, 2015) require a high level of input data, and
47 high-resolution soil maps are only available for selected areas, hindering their large-scale application (Vega-Nieva et al.,
48 2009; Kristensen et al., 2019). Therefore, researchers have turned to topographic modelling as a more promising approach
49 (Lidberg et al., 2020; White et al., 2012), as it requires only digital elevation models (DEM), which are increasingly available
50 for most parts of Europe (Hoffmann et al., 2022; Guo et al., 2017). One topographic index that has been extensively studied
51 is the "depth-to-water" (DTW) concept, originally developed and tested at the University of New Brunswick by Meng,
52 Ogilvie, and Arp, as described by Murphy et al. (2007; 2009). The DTW concept calculates flow lines across areas of interest
53 by determining a flow accumulation and selecting lines that originate at a set threshold of accumulated upstream contributing
54 areas. Using a cost function that considers the cell-to-cell slopes, the vertical distances from each cell within a raster to the
55 nearest simulated flow line are ascertained. DTW is well documented (White et al., 2012; e.g. Vega-Nieva et al., 2009; Murphy
56 et al., 2011).

57 Previous research has shown that the DTW index performs relatively well in predicting wet areas in forested formerly
58 glaciated landscapes compared to other indices (Ågren et al., 2014; Larson et al., 2022). Recent studies have explored further
59 developments in moisture prediction by utilizing machine learning algorithms applied to a variety of freely available data and
60 diverse retrieved information, including different topographic indices calculated on DEMs. Ågren et al. (2021) used 28
61 topographic predictor variables in an eXtreme Gradient Boosting model (Chen et al., 2021) to predict soil moisture across the
62 entire Swedish forest landscape at high resolution (2x2 m). Although topographic modelling approaches are widely used, they
63 often fail to adjust to seasonal changes in soil water regimes. Static maps may not adequately represent temporal occurrences
64 of flow lines, wet fields, or water-saturated soils. To address this issue, the DTW concept offers a potential solution, enabling
65 the calculation of different scenarios ranging from 'very dry' or 'frozen' to 'wet' soil conditions. However, selecting the most
66 accurate DTW scenario requires high expertise (Leach et al., 2017: 5434; Lidberg et al., 2020), and mistakes can lead to
67 reduced accuracy and result in potential soil damages that could be avoided.

68 Therefore, we believe that the next crucial step in soil moisture modelling is to incorporate a temporal component that enables
69 the prediction of rasters for any given time and area. One approach to achieve this was designed by Schönauer et al. (2022),
70 who developed a spatiotemporal prediction model. Dynamic satellite-based retrievals of soil moisture with coarse spatial
71 resolution (Soil Moisture Active Passive Mission) were combined with high-resolution but static topographic maps. This
72 resulted in improved performance in predicting moisture values across time-series conducted on sites in Finland, Germany,

73 and Poland. The incorporation of a dynamic component into the prediction model enabled reflection of the current overall
74 moisture conditions on the study sites. This allowed to calculate daily prediction grids that could support forestry practice and
75 enable the guidance of machine operators on sites to avoid traffic on wet areas susceptible to damages. However, a validation
76 of predicting rut depth by models of this kind has not been facilitated yet.

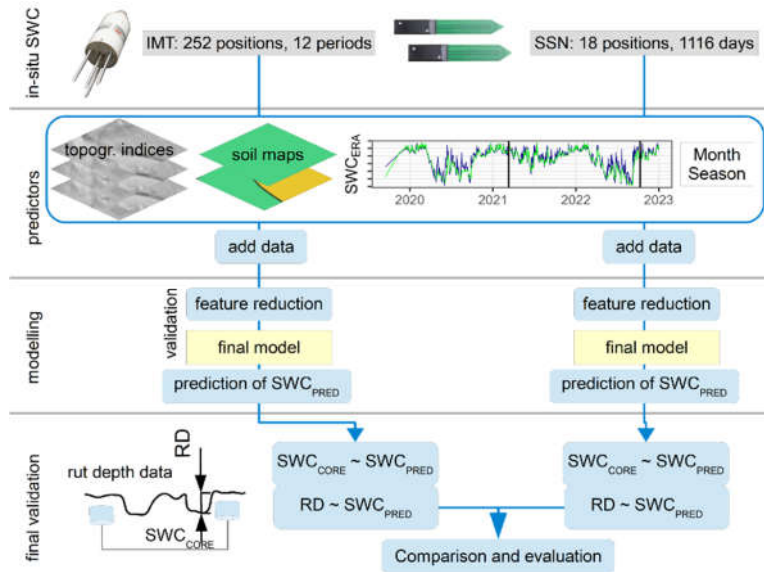
77 The effectiveness of soil moisture modelling, whether based on static or dynamic independent variables, is ultimately
78 constrained by the quality of the dependent variable, which in this case is in-situ soil moisture. Manual measurements of soil
79 moisture have been conducted in numerous studies using different devices, such as hand-held time-domain reflectometry
80 sensors (Kemppinen et al., 2018; Uusitalo et al., 2019) or impedance measuring techniques (e.g. Schönauer et al., 2021b).
81 Despite the potential inaccuracies associated with these techniques (Walker et al., 2004; Francesca et al., 2010), they offer
82 significant advantages in terms of flexibility, scalability, low investment costs, and minimal maintenance. Another option is
83 the use of continuously measuring sensor networks (e.g. Oliveira et al., 2021), which can provide relatively reliable
84 measurements but with limited spatial coverage due to the high costs of installation and maintenance.

85 In this study, we built upon the approach developed by Schönauer et al. (2022) by incorporating additional data sources,
86 including additional topographic indices, soil maps, and soil moisture retrievals from ERA5-Land for two soil depths. The
87 study also used two types of data sources for soil moisture measurements: manual measurements using a handheld moisture
88 meter, and data from two continuously measuring sensor networks. We argue that manual measurements are simpler and can
89 be applied to larger areas, while sensor networks are more expensive and limited to chosen positions.

90 The study had two main objectives: 1. to train soil moisture models using the two individual data sets (manual measurements
91 and sensor networks) and evaluate their prediction performance, and 2. to select the best combination of predictor variables
92 (e.g. topographic indices, ERA5-Land values) using a repeated cross-validation approach and compare the best models with
93 rut depth data obtained during four trials using a forwarder.

94 **2 Material and Methods**

95 To model soil water content (SWC), random forest models were trained using two separate datasets: manual in-situ
96 measurements using an impedance measuring technique (IMT) and continuously measuring soil sensor networks (SSN). To
97 both datasets we added predictor variables derived from topographic indices (e.g. depth-to-water, topographic wetness index),
98 soil maps, SWC estimates from the ERA5-Land campaign (SWC_{ERA}), and numerical values for date (month and season). We
99 performed cross-validation and reduced features stepwise to choose the best-performing model. Subsequently, the two final
100 models (for IMT and SSN) were used to predict SWC for the positions and dates of different field trials with a forwarder.
101 During these field trials, rut depth data was captured, and compared to the predictions from the final SWC-models (Figure 1).



102

Figure 1: Soil water content (SWC, [%]) was predicted using models trained on two datasets: in-situ measurements (IMT) and soil sensor networks (SSN). Input variables included topographic indices, soil type data, SWC estimates from ERA5-Land (SWC_{ERA}), and date values. Through cross-validation, we selected the final models, used to predict SWC_{PRED} for various positions and dates during trials with a forwarder. Model estimates were compared with in-situ SWC_{CORE} and rut depth (RD, [cm]).

103

2.1 Study sites

104

The data acquisition of volumetric SWC [%] and the trials with a forwarder were conducted in two forest stands located near the city of Arnsberg in North Rhine-Westphalia (Figure 2). The forest stands were situated at an altitude of approximately 250 m on common soil types such as Cambisol and Stagnosol on Claystone and Sandstone from Devon and Carbon (Table 1).

105

106

107

Table 1. Characteristics of the study sites, where soil water content was captured and field trials with a forwarder were performed.

Site	Coordinates in WGS84		Dominant soil types	Humus form	Slope [%]	Canopy
	x	y				
A	8.039	51.406	Cambisol - Stagnosol	Mesomull	15-30	<i>Fagus sylvatica</i> , <i>Quercus spp.</i> , <i>Pinus sylvestris</i>
B	8.024	51.473	Stagnosol	Mull	1-7	<i>Fagus sylvatica</i>

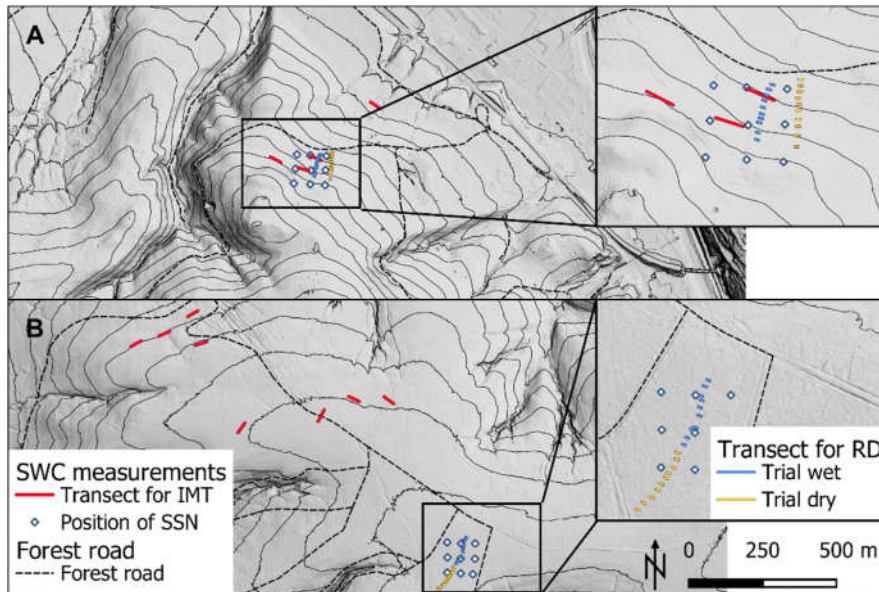


Figure 2: The map indicates the locations of two experimental areas on a hill-shaded digital elevation model with 10 m contour lines; Site A (A, coordinates x, y in WGS84: 8.039, 51.406) and Site B (B, coordinates: 8.024, 51.473), which were used for collecting time-series data on soil water content (SWC). SWC was measured using a handheld soil moisture meter (impedance measuring technique, IMT) along transects (red lines), each containing 21 measuring positions (2 m spacing). In addition, a soil sensor network (SSN) was used to continuously capture SWC at 18 positions (white rhombus). The map also indicates the locations of 40 transects (in crop-outs) used for measuring rut depth (RD) during relatively wet conditions (Trial_{WET}, blue lines) and drier conditions (Trial_{DRY}, orange lines).

108

109 2.2 Soil moisture models

110 2.2.1 In-situ soil moisture

111 Two sets of in-situ data of soil moisture were used: 1. Manual measurements of SWC were performed using a HH2 Moisture
 112 Meter (Delta-T Devices Ltd, England), which applies Impedance Measuring Technique (i.e. ‘IMT’) (Eijkelpamp Agrisearch
 113 Equipment, 2013). 2. Data from a continuously measuring Soil Sensor Network (i.e. ‘SSN’).

114 The IMT data used for this study were previously used for the validation by Schönauer et al. (2022) and consisted of 12
 115 measuring transects. The transects were placed in various positions in broadleaved forests, known to be temporarily wet or
 116 sensitive for machine traffic, with each transect having a length of 40 m. SWC was measured with a spacing of 2 m along the
 117 transects. To measure SWC, measuring rods of 60 mm length were vertically inserted into the soil after removing the humus
 118 layer. The measurements were taken almost monthly between September 2019 and October 2020 (Figure 3B). The IMT data
 119 consisted of 2,184 observations. Overall, this dataset offers a relatively high level of spatial granularity, with 252 measuring
 120 positions. However, the temporal resolution of the data is relatively low, with only monthly measuring campaigns conducted.
 121 The SSN was launched in December 2019 and its data was obtained from continuously measuring SMT100 sensors
 122 (TRUEBNER GmbH, Germany), placed on two sites, each having 9 positions with a spacing of 50x50 m. At each position,
 123 two sensors were placed at a depth of 10 cm in the mineral soil, with a temporal resolution of 15 minutes. The data from these
 124 sensors were averaged for each position and each of the 1,116 days captured (data until 2022-12-31 was included), resulting
 125 in a total of 16,351 observations after omitting all missing values. While this data set provides a high level of temporal
 126 granularity, it suffers from a low level of spatial granularity due to the limited number of positions sampled.

127 To enable the incorporation of seasonal effects in the modelling approaches, we transformed the date of each measurement

128 into numeric vectors, resulting in the variables Month and Season. The coding used for Season was as follows: 1 for March,
129 April, and May; 2 for June, July, and August; 3 for September, October, and November; and 4 for December, January, and
130 February.

131 To enable the creation of spatiotemporal data, the positions of all measuring locations were captured using post-processed
132 signals from a GNSS device (Trimble R2 RTK Rover, Trimble, Colorado, USA). This data was then fused with a range of
133 topographic indices. To achieve this, values of several topographic indices were extracted at each measuring position of IMT
134 and SSN.

135 **2.2.2 Topographic indices**

136 For calculating topographic indices, we used a freely available digital elevation model (DEM), as provided by the
137 Bezirksregierung Köln (2020). The resolution of this model was 1x1 m, with a vertical accuracy of ± 0.2 m. Using the free
138 programming language R (version 4.0.2, R Core Team, 2023) and RStudio (version 2022.07.2, Posit PBC, Massachusetts,
139 USA), along with the package "rgrass" (Bivand, 2021) to utilize GRASS GIS (Awaida and Westervelt, 2020) commands in
140 the R interface, the command 'r.hydrodem' was used to 'remove all sinks' (Flags: -a) from the DEM. Thereafter, we calculated
141 depth-to-water (DTW) maps. To generate these maps, we followed the script by Schönauer and Maack (2021) and used flow
142 initiation areas (FIA) of the following sizes 0.25 ha (DTW025), 1.00 ha (DTW1), and 4.00 ha (DTW4), which account for
143 different overall soil moisture conditions. A smaller FIA results in a DTW map for wetter conditions, as the network of
144 simulated flow lines expands, while a larger FIA represents drier conditions. For further details, refer to Murphy et al. (2009;
145 2011).

146 The Topographic Wetness Index (TWI) represents the tendency for water to accumulate at any point in the catchment (Quinn
147 et al., 1991), while the stream power index (SPI) represents the power of water flow at any point in the catchment and the
148 gravitational forces that move water downslope (Moore et al., 1991). To compute TWI, we used the 'r.watershed' command
149 in GRASS GIS, as conceived by Sørensen and Seibert (2007). TWI was calculated as $\ln(\alpha/\tan(\beta))$, where α is the cumulative
150 upslope area draining through a point per unit contour length, and $\tan(\beta)$ is the local slope angle. SPI was calculated as $\alpha * \tan(\beta)$ (Moore et al., 1991). Flow Accumulation, representing the absolute amount of overland flow passing through each cell
152 was also included as a variable. TWI, SPI, and Flow Accumulation were calculated on an aggregated DEM with a spatial
153 resolution of 15x15 m. This resolution has been shown to exhibit a stronger correlation with SWC, and can be assumed to be
154 more robust (Ågren et al., 2014), as observed in prior work where resolutions ranging from 1 to 20 m were tested (data not
155 shown). In addition, we calculated the variable Slope [$^\circ$] using the R-package 'raster' (Hijmans, 2020).

156 **2.2.3 Soil maps**

157 Soil maps of North Rhine-Westphalia were originally generated at a scale of 1:5,000 from forest site surveys. We included
158 soil type information (Soil05) for the analysis. While these maps are not available across the entire region of North Rhine-
159 Westphalia, they were provided for the study sites by the Geological Survey of North Rhine-Westphalia. By contrast, soil
160 maps with a scale of 1:50,000 are available for the entirety of North Rhine-Westphalia (Soil50).

161 **2.2.4 Temporal soil water content from ERA5-Land**

162 ERA5-Land is a global reanalysis dataset providing hourly estimates of meteorological variables at a spatial resolution of 9x9

163 km, including soil moisture [$\text{m}^3 \text{m}^{-3}$] at the top soil layer (0-7 cm, 'layer 1' (L1)) and at a depth of 7-28 cm ('layer 2' (L2)).
164 ERA5-Land data is retrieved by assimilating satellite and atmospheric forcing (Muñoz-Sabater et al., 2021).
165 We opted for ERA5-Land retrievals to address the temporal component of SWC, as this dataset offers a dependable
166 representation of soil moisture values and their variations across global regions, rendering it suitable for various geophysical
167 applications (Lal et al., 2022). Additionally, this decision is grounded on two key assumptions: 1. The spatial variability of
168 SWC is relatively low compared to its temporal variability. 2. The spatial extent of our measurement locations is small and
169 cannot be adequately captured by satellite-based Earth observation data. Even Sentinel-1, a mission within the Copernicus
170 Programme by the European Space Agency renowned for supporting high-resolution (1x1 km) surface soil moisture product
171 generation (Peng et al., 2021), would have limited utility in providing spatial information for our study sites. For instance, the
172 maximum distance between rut depth transects (Section 2.3.2) was 200 m. Furthermore, since Sentinel-1 focuses on surface
173 soil moisture using the C-Band, we assume that ERA5-Land's soil moisture estimates for deeper layers might offer a better
174 fit for our data, as suggested by similar findings presented by Fjeld et al. (2024).
175 We utilized the API provided by CDS (Copernicus Climate Change Service, 2019) and the R-package 'ecmwf' (Koen Hufkens
176 et al., 2019) to download daily grids (at 14:00 UTC) of layer 1 and 2. The downloaded data covered both the whole time span
177 of our data and the two measuring sites. Both sites were situated in one 9x9 km raster cell of the ERA5-Land. The land cover
178 for this cell was derived from Bezirksregierung Köln (2023), showing that open land (e.g. grassland, crops) dominated with
179 52% of the total cover, whereas forests occurred on approximately 31% of the cell size, followed by 12% coverage from
180 infrastructure, 3% loose material, and 2% water bodies.
181 After downloading the data, we stacked the daily grids and extracted the corresponding values at each measuring position,
182 giving $\text{SWC}_{\text{ERAL1}}$ and $\text{SWC}_{\text{ERAL2}}$.
183 All data, the topographic information, soil types, numerical values of date and the dynamic variables from ERA5-Land were
184 merged with in-situ data, either IMT or SSN.

185 **2.2.5 Modelling**

186 The modelling approach described here was applied separately for both data sets, IMT and SSN (and for both datasets
187 combined).
188 Initially, we fitted a linear model with SWC as the dependent variable and $\text{SWC}_{\text{ERAL1}}$, $\text{SWC}_{\text{ERAL2}}$, Month, Season, DTW025,
189 DTW1, DTW2, DTW4, Slope, TWI, SPI, Accumulation, Soil05, and Soil50 as the independent variables. We then used this
190 linear model to check the data for autocorrelations and subsequently eliminated variables with a variance inflation factor > 10
191 through an iterative process, reducing one variable at a time. Also, the feature selection according to the Boruta algorithm
192 (package 'Boruta', Kursa and Rudnicki, 2010) was applied.
193 We then trained random forest models (Breiman, 2001), repeatedly reported as efficient in predicting complex data (Cavalli
194 et al., 2023; Carranza et al., 2021; Kemppinen et al., 2018), using the 'ranger' package (Wright and Ziegler, 2017) with a 10-
195 fold cross-validation with 5 repetitions. For each of the 50 models in the validation of one configuration, we noted the mean
196 of Kendall's coefficient of correlation τ (since different sample sizes occurred) of the random forests and the representative
197 standard deviation. In addition, the least important variable according to impurity and its frequency within the 50 validation
198 sets were traced. The variable noted most frequently as least important was then removed, and a new cross-validation was
199 performed on $\text{SWC} \sim (n-1)$ variables, with n being the number of predictors in the model trained previously. This process was

200 repeated until only one predictor variable remained.
201 To avoid temporal autocorrelations at the measuring positions, positions IDs were used to select the folds of the cross
202 validations.

203 **2.2.6 Selection of the final model**

204 To select the final random forest model for each data partition, we examined the maximum τ values obtained and multiplied
205 them by 0.99 (according to Hauglin et al. (2021)). This was done to penalize the use of an unnecessarily high number of
206 predictor variables. We selected the model with the least number of predictor variables within this 1%-range as the final
207 model. The final models (built on IMT and SSN data) were then used to predict rasters of SWC_{PRED} , which were visually
208 evaluated. Subsequently, the outputs of the final models were compared to rut depths and SWC at the machine operating
209 trails.

210 **2.3 Data from field trials with a forwarder**

211 **2.3.1 Rut depth (RD)**

212 During the field trials conducted in two forest stands at two seasons, a fully loaded forwarder (John Deere 1210G, 8-Wheel
213 model, total mass of 28 Mg (18 Mg machine weight + 10 Mg loading)) was used. The first trial was conducted on section 1
214 of an existing machine operating trail on 2021-03-11, during generally wet conditions ($\text{Trial}_{\text{WET}}$). The second trial was
215 conducted on subsequent section 2 of the same machine trail on 2022-10-11, during drier conditions ($\text{Trial}_{\text{DRY}}$) (Figure 2, Site
216 B), or in close proximity of section 1 (Site A), as there the machine trail was not long enough for both sections.

217 The four trials were positioned near the sensors of the SSN (Figure 2) and, in the case of Site A, near the IMT measuring
218 transects. On Site B, the IMT transects were at a distance of 530 m to 1300 m. Moreover, there is a temporal lag between the
219 IMT measuring campaigns and the field trials (Figure 3). This discrepancy stems from the IMT data being collected as part
220 of a separate research project.

221 The 8-wheel machine trafficked section 1 and 2 of both operating trails, and made four passes. Before the first machine pass,
222 the initial surface was captured along 10 perpendicular transects on each of the four sections. These 4 m wide transects were
223 placed and marked permanently with inserted wooden pegs. The same pegs were used to position the beam, which served as
224 the reference height to measure profiles along each transect. Into this beam, metric scales were inserted with a spacing of 10
225 cm in between, to note the distance between the surface and the beam to the nearest cm. These measured distances (D_0 , [cm])
226 describe the surface along the transect on already existing machine operating trails, prior to the trial conducted in this study.
227 The same procedure was repeated after the fourth consecutive machine passes, giving D_4 [cm].

228 Next, the differences between D_0 and D_4 were calculated at each of the 41 measurements (10 cm spacing over 4 m) along a
229 transect. The maximum value of these differences, measured at the left or right machine track, was used to determine rut depth
230 (RD, [cm]). We used average values of both tracks to prevent pseudo replicates, since intraclass correlation coefficient was
231 high (0.83), when left and right tracks were integrated separately. Moreover, mean and maximum values of rut depth were
232 highly correlated (adj. $R^2 = 0.96$).

233 Four of the 40 transects for measuring RD were not ascertainable as the forwarder destroyed the wooden pegs that positioned
234 the reference beam. In $\text{Trial}_{\text{WET}}$, conducted in March 2021, SWC_{ERAL1} and SWC_{ERAL2} showed a soil moisture level of 39%.
235 At Site A, the measured RD was 10.3 ± 1.9 cm, while at Site B, the RD was 12.7 ± 5.5 cm, with the highest value of RD recorded

236 after 4 passes, with a depth of 21.5 cm. In Trial_{DRY}, conducted in October 2022, the soil water content from ERA5-Land was
237 32%. At Site A, the measured RD was 3.5±1.7 cm, and at Site B, the RD was 4.3±1.2 cm. Comparisons of RD with DTW
238 and TWI are given in Figure C1.

239 2.3.2 Soil water content at the rut depth transects (SWC_{CORE})

240 Volumetric soil moisture content was captured outside the 1st, 4th, 7th and 10th transect of each section, with a distance of 1 m
241 to the left and right track, at a depth of 10-15 cm. This water content was determined using 100 cm³ cores taken with an
242 undisturbed core sampler, with three replicates at each measurement. SWC_{CORE} was calculated according to equation (1):

$$SWC_{CORE}[\%] = \frac{M2 - M1}{M1} * 100 \quad (1),$$

243 with M2 being the fresh mass of the soil taken with undisturbed cores and M1 being the mass after drying the samples in oven
244 with 105 °C, until mass constancy was reached.

245 Measurements of RD and SWC_{CORE} were georeferenced using the GNSS devise and complemented with all the predictor
246 variables, as described above.

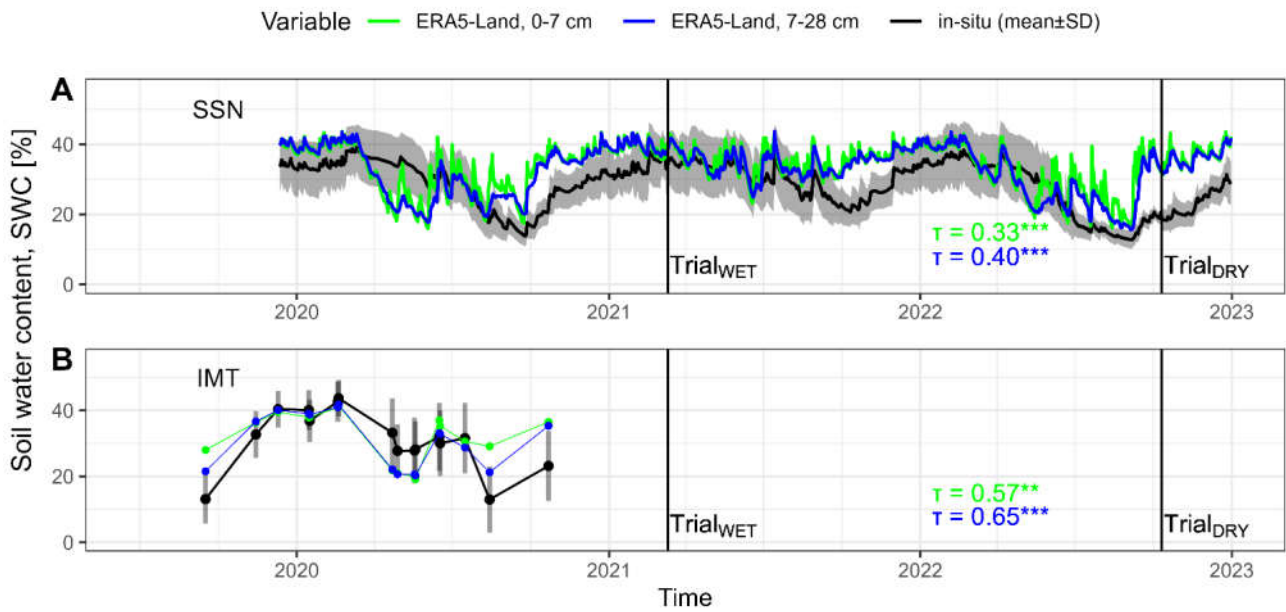
247 2.4 Comparisons between model predictions and RD or SWC_{CORE}

248 For the ‘testing on rut depth data’ (Figure 1), values of SWC_{PRED} were compared to RD or soil water content, captured through
249 undisturbed cores along the transects, SWC_{CORE}. The predictor variables from the rut depth dataset were used to predict
250 SWC_{PRED} by means of the final random forest models created in the soil moisture modelling. Since the goodness-of-fit
251 between in-situ values of RD or SWC_{CORE} and SWC_{PRED} was to some degree sensitive to the seed set during modelling, we
252 repeated the predictions ten times and used average values to receive robust estimates of SWC_{PRED}. To test the correlations
253 between paired samples of SWC_{CORE} or RD and SWC_{PRED}, Kendall's rank correlation was used. We illustrated the
254 corresponding p-values as follows: ‘***’ for p<0.001, ‘**’ for 0.001-0.01, ‘*’ for 0.01-0.05, (‘*’) for 0.05-0.10 and ‘ns’ for p-
255 values being higher than 0.10. Root mean squared error (RMSE) and mean squared error (MSE) were calculated according to
256 Hamner and Frasco (2018). Values are given as mean±standard deviation.

257 3 Results

258 3.1 Soil water content

259 The mean value of SWC, measured using a handheld moisture meter (IMT), varied between 13.0±10.0% in August 2020 and
260 43.2±5.95% in February 2020 (Figure 3). Daily mean values obtained from soil sensor networks (SSN) were similar to those
261 obtained from IMT, ranging from 13.8±2.90% in September 2020 to 39.1±6.66% in March 2020, in the period that
262 corresponds to the one covered by IMT. The driest conditions were observed in September 2022, with a daily mean SWC of
263 12.7±2.55%. Overall, the results suggest that IMT and SSN provide comparable estimates of SWC, with the latter providing
264 higher temporal resolution at a low spatial granularity.



265
266

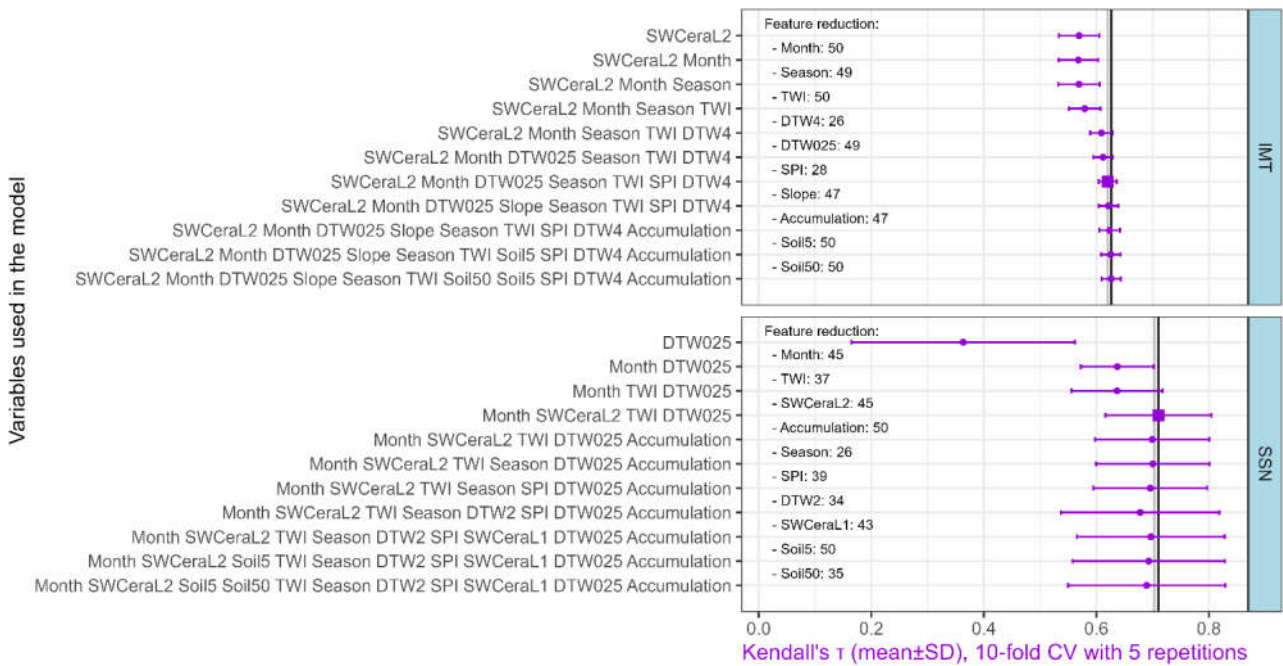
Figure 3: Time series of soil water content (SWC) measured using a soil sensor network SSN (A) with 18 measuring positions on two sites and manual measurements, using impedance measuring technique IMT (B) conducted on 252 positions (black lines/points show daily mean values, grey shading/bars show standard deviation for each day). SWC retrievals from ERA5-Land are shown as a blue line/point (0-7 cm vertical resolution, as available from Copernicus Climate Change Service (2019)) and a green line/point (7-28 cm vertical resolution). The goodness-of-fit between daily means of measured SWC and ERA5-Land retrievals is reported using Kendall's rank correlation coefficient (τ). Vertical lines indicate the dates of the trials when a forwarder conducted four passes at existing machine operating trials.

267 3.2 Soil moisture models

268 The positions IDs were used to select the 10 folds for cross-validation. However, the dataset SSN had only 18 measuring
269 positions (where SWC was measured on 1116 days), resulting in relatively high deviations of Kendall's τ of the random
270 forests. The most important feature for this dataset was given by DTW025, although the resulting quality was low, with τ of
271 0.363 ± 0.198 . By adding the temporal component Month, the τ improved to 0.637 ± 0.065 , which had the lowest standard
272 deviation for the repeated folds. The final model for this dataset included the temporal variables Month and SWC_{ERA5L2} , as
273 well as the topographic predictor variables TWI and DTW025 (Figure 4). The resulting τ was 0.710 ± 0.095 , revealed through
274 the cross-validation.

275 For the IMT partition, which had a low temporal but high spatial resolution, the most important feature was the temporal
276 information SWC_{ERA5L2} , leading to a τ of 0.569 ± 0.036 . The final model had an τ of 0.620 ± 0.016 , including the predictor
277 variables SWC_{ERA5L2} , Month, Season, and DTW025, TWI, SPI and DTW4.

278 The main outputs when both datasets were combined can be seen in Figure A1.

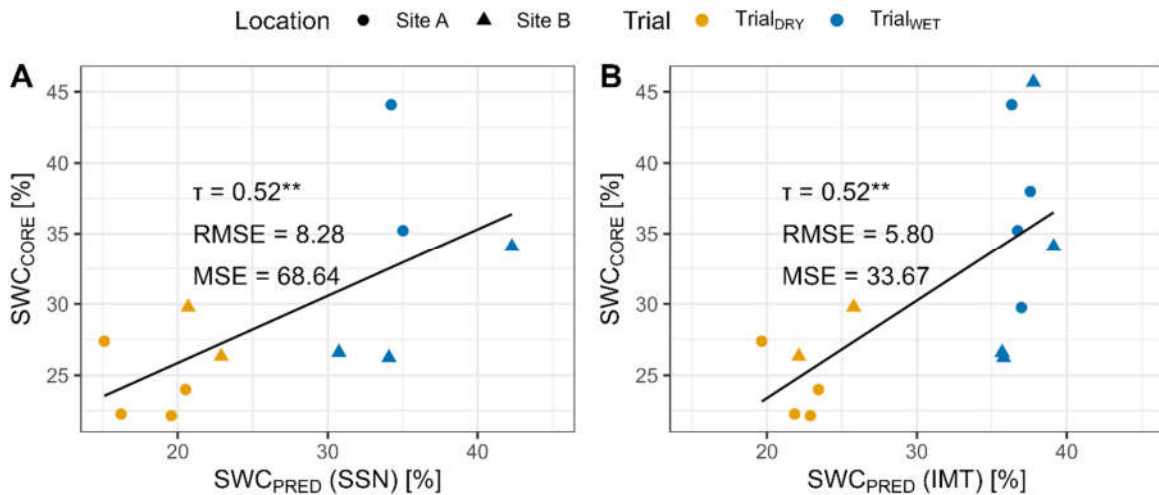


279

Figure 4: Soil water content (SWC) was modelled by random forests (RF), and evaluated by a repeated 10-fold cross validation (CV). Mean values and standard deviation of resulting values of the Kendall rank correlation coefficient τ during the CV are shown. A stepwise elimination of the least important variable was performed, and the frequency of this variable over all models is provided (“Feature reduction”). The vertical lines indicate the maximum value of τ (black) and the 99% of the maximum (grey), to select final models (squares). Variables used are described in section 2.

280 3.2.1 Comparisons of SWC_{CORE} with SWC_{PRED}

281 The final random forest models of both, the IMT and SSN dataset, were used to calculate SWC_{PRED} on the predictor variables
 282 of the rut depth data, including SWC_{CORE} measured at the outside of a subsample of the measuring tracks by undisturbed
 283 cores. The comparison between SWC_{CORE} and SWC_{PRED} values predicted by the final random forest models of both datasets
 284 (SSN and IMT), revealed a significant association (Figure 5).



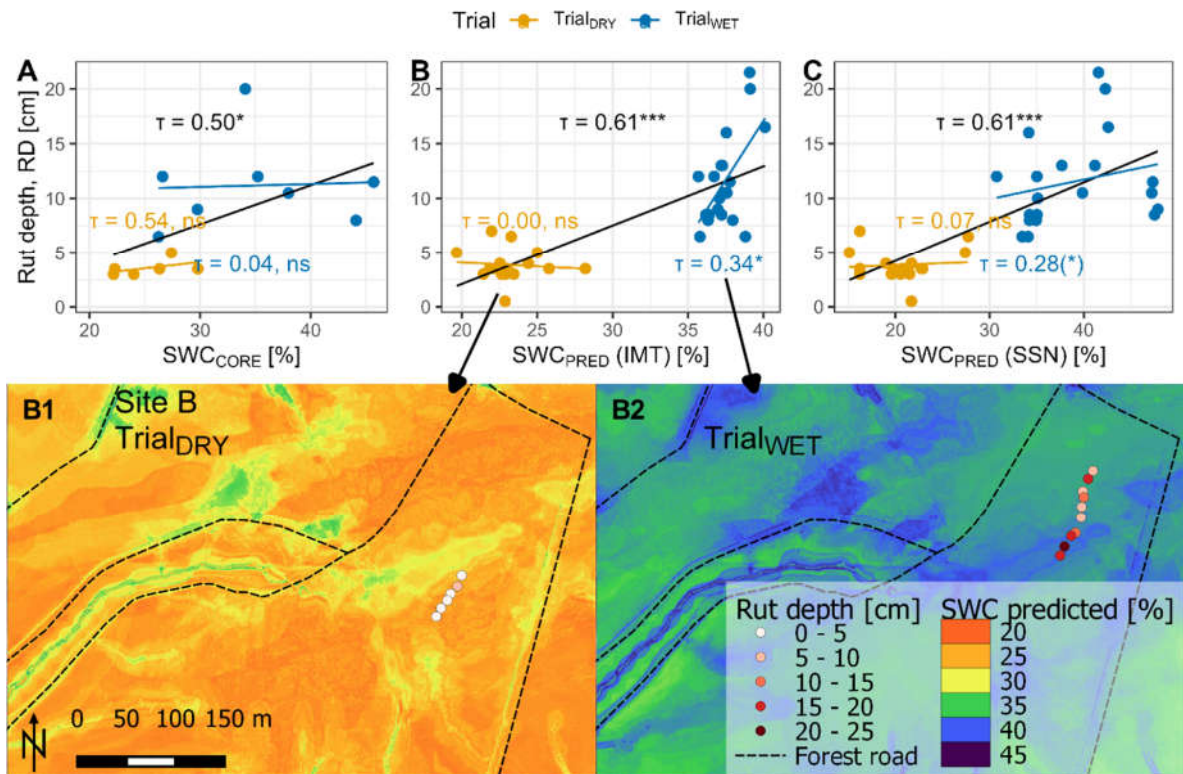
285

Figure 5: Soil water content was measured during two trials with a forwarder along a machine operating trail ($n=14$), using 100 cm^3 undisturbed cores (SWC_{CORE}), and compared to values predicted (SWC_{PRED}) by a model trained data from a continuously measuring soil sensor network (SSN, A), or manual measurements with a handheld moisture meter (IMT, B). Correlations were evaluated

using Kendall's τ and significance levels are indicated by *** for $p < 0.001$, ** for 0.001-0.01, * for 0.01-0.05, (*) for 0.05-0.10, and 'ns' for $p > 0.10$.

286 **3.3 Comparisons of RD with SWC_{CORE} and SWC_{PRED}**

287 RD was positively correlated with SWC_{CORE} when both trials with different moisture conditions were included in testing
 288 (Figure 6A). However, when each trial was tested separately, no correlation between RD and SWC_{CORE} was observed (Figure
 289 B1). Compared to the correlation between RD and SWC_{CORE} , modelling outputs SWC_{PRED} proved to be a better predictor of
 290 rut depth, particularly for Trial_{WET}. The final models that were selected for both datasets produced a Kendall's τ of 0.61 (for
 291 IMT, Figure 6B, and SSN, Figure 6C), when comparing RD of the four trials with the corresponding SWC_{PRED} . Although the
 292 R^2 values for these models were in similar range (0.620 for IMT and 0.549 for SSN), we chose to use Kendall's τ since different
 293 sample sizes were involved in the analysis. This was particularly relevant for comparing RD with SWC_{PRED} for each Trial
 294 separately. While no correlation could be found for Trial_{DRY}, correlations were found for Trial_{WET}, with Kendall's τ of 0.344
 295 ($p=0.037$) and 0.281 ($p=0.090$), for the final models trained on IMT and SSN, respectively (Figure 6B,C). Yet, these
 296 correlations seem fragile, as a difference of a few percent of predicted SWC_{PRED} (IMT) is associated with the range of RD
 297 between 6.5 and 21.5 cm. Moreover, when analysing the sites separately, a vague trend between SWC_{PRED} and RD could be
 298 observed, but without showing significant correlations (Figure B1).
 299 Since the final model trained on IMT data performed slightly better in Trial_{WET} compared to the model trained on SSN data
 300 (Figure 6), we chose the IMT model for the generation of prediction rasters for the days of interest (Figure 6B1,B2).
 301



302 Figure 6: Rut depth (RD) was determined after four passes of a forwarder, driving on two Sites, during two conditions (WET and DRY). RD was compared to SWC values, determined for undisturbed soil cores (A) and SWC values predicted by a random forest model trained on manually obtained IMT measurements (B, see Figure 1) and predicted by a model trained data from a continuously

measuring soil sensor network (SSN, C). Correlations were evaluated using Kendall's τ . The correlation of all values is given in black, blue and yellow show the Trials during wet and dry conditions. Significance levels are indicated by *** for $p < 0.001$, ** for 0.001-0.01, * for 0.01-0.05, (*) for 0.05-0.10, and 'ns' for $p > 0.10$. The model based on IMT data (B) was used to calculate prediction rasters for the days of the field trials (B1, B2).

303 4 Discussion

304 4.1 Importance of predictive systems

305 Wet soils are prone to soil disturbances like the formation of deep ruts (Poltorak et al., 2018; McNabb et al., 2001), since
306 water implies a reduction of particle-to-particle bondings within the soil (Hillel, 1998), decreasing the resistance to external
307 forces. Consequently, accurate predictions of soil water content (SWC) and soil trafficability is essential for sustainable forest
308 management and cost-effective, environmentally friendly harvesting operations (Vega-Nieva et al., 2009; Mattila and Tokola,
309 2019; Picchio et al., 2020; White et al., 2012; Murphy et al., 2007; Mohtashami et al., 2017; Uusitalo et al., 2020). Topographic
310 modelling requires minimal input and the temporal variables used in the final model presented here, are freely available
311 (Copernicus Climate Change Service, 2019). A spatiotemporal model predicting SWC could improve the guidance of machine
312 operators in forest sites during harvesting operations, for example by the effective positioning of brush mats (Labelle et al.,
313 2019; Labelle and Jaeger, 2018). Practical use of static, topographic maps has already been observed in Canada and
314 Scandinavian countries (Ring et al., 2022). By incorporating a temporal aspect, the accuracy of these tools could be further
315 improved. This has the potential to enhance sustainable forest management by protecting soil and mitigating harmful sediment
316 transport (Ågren et al., 2015; Lidberg et al., 2020; Kuglerová et al., 2017; White et al., 2012).

317 4.2 Comparison to previous work on predictions of SWC

318 Since soil moisture predictions are crucial for a variety of forestry aspects, several publications have focused on this topic
319 before. For example, Lidberg et al. (2020) predicted soil moisture classes using spatial models built on topographic indices,
320 correctly classifying 73% of wet areas in a Swedish case study. Ågren et al. (2014) reported accurate predictions for 87-92%
321 of observations by comparing soil moisture classes to DTW maps. Larson et al. (2022) used data from the Krycklan catchment
322 and found an accuracy of 84% when comparing moisture classes to the recently developed 'SLU soil moisture map' (Ågren
323 et al., 2021). However, these validations were based on static topographic maps. One attempt to make such static maps
324 dynamic was realized within the DTW concept, which can be customized to calculate various scenarios to adjust to general
325 moisture conditions (e.g., flow initiation areas of 0.25, 1, and 4 ha for wet, moist, and dry conditions, respectively), but
326 selecting the most appropriate scenario during practical use can be a challenging task that requires significant expertise (White
327 et al., 2012; Lidberg et al., 2020; Leach et al., 2017: 5432). To overcome this challenge, we aimed for improvement of soil
328 moisture prediction and refined the spatiotemporal approach conceived by Schönauer et al. (2022). During cross-validation
329 of IMT data from sites in Finland, Poland, and parts of the data used in this work, they reported an R^2 of 0.80. The models for
330 the present study showed an R^2 of 0.759 ± 0.136 (SSN) or 0.636 ± 0.040 (IMT), corresponding to Kendall's τ of 0.710 ± 0.095
331 or 0.620 ± 0.016 , respectively. Although this may not seem like an improvement, it should be noted that the data from German
332 sites had less explanatory power of topography for predicting SWC. For example, DTW4 alone explained SWC to a very
333 limited extent ($R^2 = 0.037^{***}$).

334 4.3 Prediction of rutting

335 Besides the comparisons of SWC with DTW maps, various studies have also investigated the capability of topographic indices
336 in predicting rutting – with conflicting outcomes. For example, Vega-Nieva et al. (2009) found that 65% of ruts deeper than
337 25 cm were located in areas with a DTW value of less than 1 m, and 93% of these ruts occurred in areas with DTW values
338 less than 10 m. Similarly, Heppelmann et al. (2022) observed a high frequency of severe rut depth in areas with DTW values
339 less than 1 m in Norway. However, Mohtashami et al. (2017) did not find evidence of such patterns in a field trial where the
340 inclusion of DTW values did not improve the accuracy of a linear model to describe the extents and degrees of rut depth on
341 machine operating trails. In agreement, Schönauer et al. (2021a) found no evidence that DTW or TWI could predict rut depth
342 in a field trial conducted in a temperate broadleaved stand. In this study, we found a significant correlation between RD and
343 DTW025 with a Kendall's correlation coefficient (τ) of -0.52***. Yet, this correlation has to be seen with caution: It is mainly
344 driven by differing ranges of RD between the two Trials, as can be seen in Figure C1A. We observed that the temporal
345 adjustments of the model based on current moisture conditions improved predictions of rutting by up-to-date SWC predictions,
346 leading to a τ of 0.61*** (Figure 6B,C). While a strong association between RD and predicted values of SWC was observed,
347 the influence of differences between the trials is evident. However, the ranges of RD for each trial were consistent with the
348 SWC predictions. In Trial_{WET}, a significant correlation between RD and SWC_{PRED} was observed (Figure 6B). We hypothesize
349 that the wetter conditions during this trial, which lead to soil destabilization (Hillel, 1998; McNabb et al., 2001), enhanced
350 the predictive power of topographic indices representing soil water distributions. For instance, DTW025 overlapped with
351 surface water in depressions, as observed in the field campaigns for Trial_{WET}.

352 In contrast, during Trial_{DRY}, no correlation was found between RD and SWC_{PRED}. SWC along the measuring sections was
353 likely below the threshold for soils to become susceptible to deformation. For example, Poltorak et al. (2018) stated that ruts
354 only occurred on soils with an SWC above 50%, whereas SWC_{CORE} at Trial_{DRY} was below 30% (Figure 5).

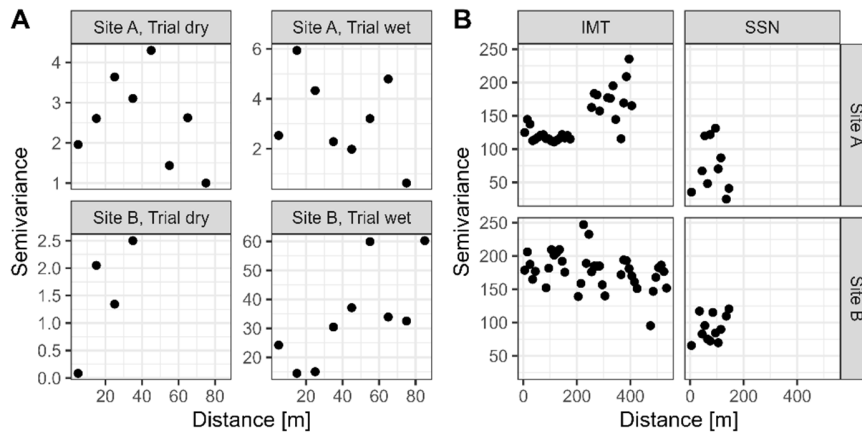
355 4.4 Description of the model

356 The best-performing model in predicting RD incorporated temporal information from SWC_{ERAL2}, Month and Season, as well
357 as spatial information from DTW025, TWI, SPI and DTW4, and was based on data from the manual measurements (IMT).
358 The IMT data was collected in close proximity to the rut depth measurements at Site A (Figure 2), or with a distance of up to
359 1.3 km at Site B. However, the spatial distance between the IMT training data and the rut depth data did not seem to be crucial
360 for the accuracy of predicting rut depth (Figure B1), since Kendall's τ between RD and SWC_{PRED} was similar for both sites.
361 Surprisingly, the correlation between in-situ SWC_{CORE}, sampled directly at the machine operating trails, showed a lower
362 explanatory power in predicting RD than SWC_{PRED}. Although an overall association was confirmed, no correlation could be
363 found when trials were analysed individually.

364 4.4.1 Temporal variaton was more important than spatial variation

365 The lacking association between RD and SWC_{CORE} on individual trials indicates that the temporal variability in soil moisture
366 between the trials was more important in this study than the spatial variability within the relatively small areas where each
367 trial was conducted. The spatial distrubution of the rut depth measurements might have been limiting in the present work. The
368 semivariogram indicates the spatial covariation of rut depth and SWC (Figure 7). While the covariation of RD in Site A is
369 indicated to be high within a range of 10 m (RD-transects were at this distance), on Site B during wet conditions, the sill of

370 the semivariogram reaches almost 40 m, which covered a high number of transects. Similarly, excluding soil information in
 371 the initial stages of feature reduction suggests homogeneous soil properties on the relatively small study area.
 372 Therefore, we have to admit, that the study design was not ideal for assessing the ability to predict rutting with a spatiotemporal
 373 model of SWC, and the results have to be considered with caution.



374

Figure 7. Semivariogram illustrating spatial autocorrelation of (A) rut depth (cm) and (B) soil water content (SWC) across the study area. Rut depth was measured during two moisture conditions, at four machine operating trail sections, allocated on two sites. The measuring transects had a spacing of 10 m. SWC was measured with handheld measuring techniques (IMT), or a soil sensor network (SSN) (Figure 2).

375 The spatiotemporal model (IMT), also supports the conclusion that spatial variations were either underrepresented by the
 376 study design or very low compared to temporal variation by nature as the temporal feature SWC_{ERA2} was selected as most
 377 important variable and the difference between the model with one predictor variable vs. the final model was small (Figure 4).
 378 Still, this slight increase in the models' quality allowed for the integration of spatial patterns and resulted in the significant
 379 but vague prediction of RD in Trial_{WET} ($\tau = 0.344^*$, Figure 6). Another indication of the integration of spatial patterns can be
 380 interpreted by the segregation of the temporal range of the IMT data (2019-2020) and the actual Trials (March 2021 and
 381 October 2022, Figure 3), indicating a generalization of spatial and temporal patterns.

382 4.4.2 Most important variables

383 In the final model (IMT), SWC_{ERA2} has been identified as the most important variable, followed by Month and Season. It is
 384 noteworthy that in the data with broader spatial coverage (i.e. IMT), in contrast to the SSN data, dynamic variables took
 385 precedence over predictor variables. Surprisingly, when modelling SSN data, characterized by high temporal resolution and
 386 low spatial resolution, DTW025 remained the most influential variable. One might have anticipated the opposite, expecting a
 387 topographic index to play a central role in modelling IMT data, and dynamic SWC_{ERA} variables dominating the modelling of
 388 SSN data.

389 We presume that the low spatial variations of SWC in comparison to temporal variations, inadequately represented by the
 390 provided topographic information, may have contributed to this unexpected outcome. Furthermore, the wider spatial coverage
 391 in the IMT data likely resulted in more robust averages of SWC, leading to a stronger correlation with the coarse spatial data
 392 of ERA5-Land (9x9 km). On the contrary, the SSN data, originating from areas with a size of 100x100 m and known for their
 393 temporal wetness, could explain the heightened importance of DTW025. Some sensors might have measured constant water
 394 saturation, thereby inflating the explanatory power of topographic information. These assumptions are speculative, and further

395 research in this direction is warranted.

396 In the feature reductions of IMT and SSN data (Figure 4), SWC_{ERA2} (7-28 cm soil depth) dominated over SWC_{ERA1} (0-7
397 cm). This aligns with in-situ measurements of SWC by the SSN, conducted at a soil depth of approximately 10 cm (Figure
398 3A). Even for the IMT data, where SWC was measured in the top 6 cm of soil, SWC_{ERA2} yielded a better goodness-of-fit
399 compared to SWC_{ERA1} (Figure 3B). We hypothesize that the prevalence of open lands as the dominant land cover form in
400 the ERA5-Land raster cell (section 2.2.4) contributed to the superior fit of SWC_{ERA2} . Grasslands typically exhibit higher
401 temporal heterogeneity of soil moisture compared to forests (James et al., 2003). This temporal heterogeneity tends to decrease
402 with deeper soil layers (Tromp-van Meerveld and McDonnell, 2006). Therefore, the stronger correlation between SWC_{ERA2}
403 and SWC, as well as its higher importance within the random forests, seems reasonable. The disparity between SWC_{ERA} and
404 in-situ SWC can be attributed to the high transpiration rates in forests, as opposed to grass (Kelliher et al., 1993).

405 **4.5 Further developments**

406 The terrain data was derived from a digital elevation model, which is increasingly available for the entire Europe (Hoffmann
407 et al., 2022), while the dynamic variables are based on data and retrievals from ERA5-Land, which are freely available up to
408 a few days ago. These inputs would allow for automated mapping of current soil water content, which could be made
409 accessible to forestry stakeholders. Recent developments also show a pathway to integrate medium and long range weather
410 forecasts into trafficability predictions, as conceived by the Finnish Meteorological Institute (2023). Both, recent as well as
411 forecasting predictions can lead to improved soil protection, higher efficiency of timber harvesting (Suvinen and Saarilahti,
412 2006), and a new stage of sustainable forest management (Campbell et al., 2013; D'Acqui et al., 2020; Uusitalo et al., 2019;
413 Jones and Arp, 2019). However, it should be noted that the in-situ data of SWC originated from manual measurements, and
414 it was relatively labor-intensive to gather this amount of data. There is potential to reach appropriate accuracy even with a
415 reduced dataset - further investigation would be necessary to determine the essential input data criteria. The alternative to
416 manual measurements is given by sensor networks, which led to comparable results, but such sensor networks are expensive
417 to establish and maintain. Nonetheless, initiatives of installing sensors are emerging and additional manual measurements
418 could be conducted. In the future, forestry stakeholders who require accurate raster predictions could potentially facilitate
419 manual measurements or install sensors and provide the captured data to scientific organizations, which could deliver
420 spatiotemporal soil moisture predictions in return. The captured data could be made available for creating spatiotemporal
421 models of SWC, allowing for additional training data and daily raster predictions for new areas of interest, with various
422 scientific insights and practical applications.

423 **Conclusion**

424 In this study, we developed a spatiotemporal model that used multiple topographic indices, temporal variables, soil moisture
425 retrievals from ERA5-Land, and data from manual measurements to predict soil water content (SWC). Predicted values of
426 SWC were compared to rut depth data collected during four forwarder trials. Overall, the model performed well in predicting
427 rut depth, with a Kendall's τ of 0.61 for all trials. Yet, this result has to be considered with caution, since spatial covariation
428 was detected in parts. We hope, that this experience helps for future research, in which more attention to spatial covariation
429 on soils should be paid. Still, we believe that a dynamic prediction of SWC will help forest managers and machine operators
430 avoid wet areas, leading to more sustainable forest operations. Using freely available temporal information is a significant

431 improvement, as it enables more accurate and up-to-date predictions, which allow to make more informed decisions and avoid
432 potential hazards. Future work should focus on developing automated pathways for generating daily raster predictions of
433 SWC, and on generating reliable and comprehensive in-situ data. There is a need for more data on rutting and SWC, measured
434 with a sufficient spatial coverage, whether by manual measurements, the establishment of additional sensor networks, or by
435 automatic ways of capturing rut depth data through machines driving off-road, to cover more areas and different sites and
436 regions.

437 **Data availability**

438 The data used in this work will be made accessible via Zenodo

439 **Author contribution**

440 MS and DJ designed the experiments and MS and FH carried them out. MS developed the model code and performed the
441 simulations. MS prepared the manuscript with contributions from all co-authors.

442 **Competing interests**

443 The authors declare that they have no conflict of interest.

444 **Acknowledgements**

445 We acknowledge the financial support from the Eva Mayr-Stihl Stiftung for this work. We extend our gratitude to the
446 Geological Survey of Northrhine-Westphalia (Landesbetrieb NRW) for conducting the soil mapping on the experimental sites
447 and for their contributions to the field trials analysis. In particular, we would like to thank Dr. Heinz Peter Schrey, Dirk Elhaus,
448 Thilo Simon, and Rainer Janssen. Our appreciation also goes to the Forest Education Centre, Forstliches Bildungszentrum,
449 Zentrum für Wald und Holzwirtschaft, Landesbetrieb Wald und Holz NRW, Arnsberg, Germany, for their valuable support
450 during the fieldwork. Special thanks to Thilo Wagner and Thomas Späthe for their efforts in organizing the field trials, and to
451 Michael Schulte for operating the forwarder. ChatGPT (OpenAI, San Francisco, CA, USA) provided assistance in sentence
452 editing – all content was generated solely by the authors.

453 **Funding**

454 This work was supported by the cooperation project “BefahrGut” funded by the State of North Rhine-Westphalia, Germany,
455 through its Forest Education Centre, Forstliches Bildungszentrum, Zentrum für Wald und Holzwirtschaft, Landesbetrieb Wald
456 und Holz NRW, Arnsberg, Germany; by the Bio Based Industries Joint Undertaking under the European Union’s Horizon
457 2020 research and innovation program, TECH4EFFECT Knowledge and Technologies for Effective Wood Procurement—
458 project, [grant number 720757].

459

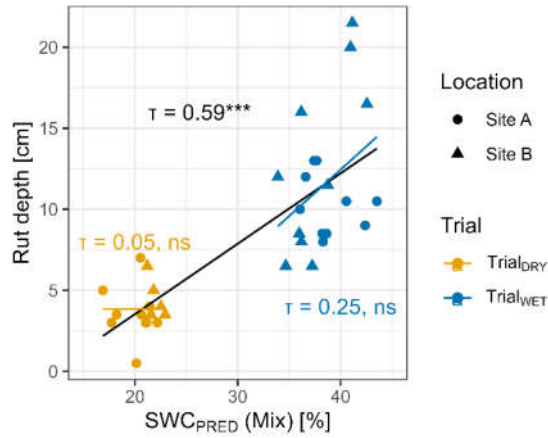
460 **5 Appendix**

461 **Appendix A**

462 To model the dataset consisting of both IMT and SSN data, the procedure described in section 2 was followed. The IMT
463 dataset was merged with a subsample of the SSN dataset, where the sample size of the SSN part was twice that of the IMT
464 dataset. This was done to prevent over-weighting of the SSN dataset. The resulting combination of IMT and SSN data was
465 called the "Mix" dataset.

466 The final model using the Mix dataset included the input variables SWC_{ERAL2} , Month, TWI, SWC_{ERAL1} , DTW025, Season,
467 DTW1 and DTW4, and achieved a τ of 0.655 ± 0.081 (which corresponded to R^2 values of 0.639 ± 0.108). Figure A1 shows
468 that the correlation between the model outputs (SWC_{PRED}) and rut depth (RD) was significant.

469 Since the models trained on the Mix dataset did not perform better than those trained on the IMT or SSN datasets, we did not
470 investigate the fused data partition any further, as one research question addressed the use of different data origins. For future
471 work, however, the fused data would provide additional information, as compared to the individual datasets.



472

Figure A1: Rut depth (RD) was determined after four passes of a forwarder, driving on two Sites (A and B), during two seasons (Trial_{WET} and Trial_{DRY}). RD was compared to SWC values predicted by a random forest model trained on data from manual measurements or captured through a continuously measuring soil sensor network ('Mix'). Correlations were evaluated using Kendall's τ and significance levels are indicated by *** for $p < 0.001$, ** for 0.001-0.01, * for 0.01-0.05, (*) for 0.05-0.10, and 'ns' for $p > 0.10$.

473

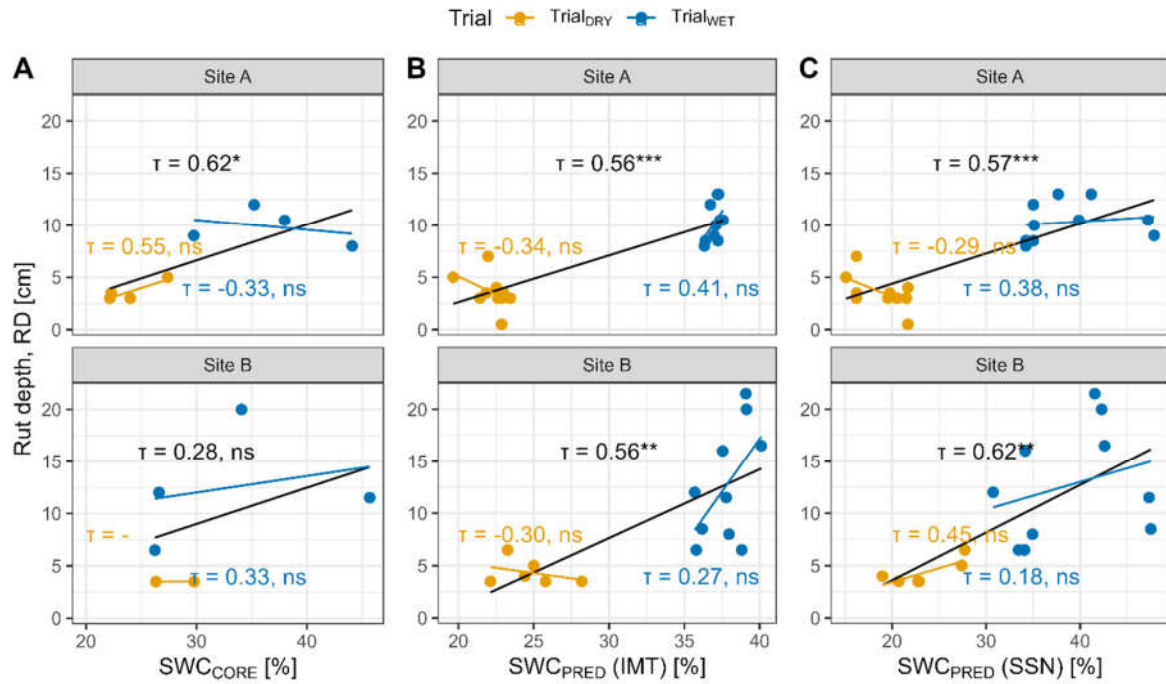
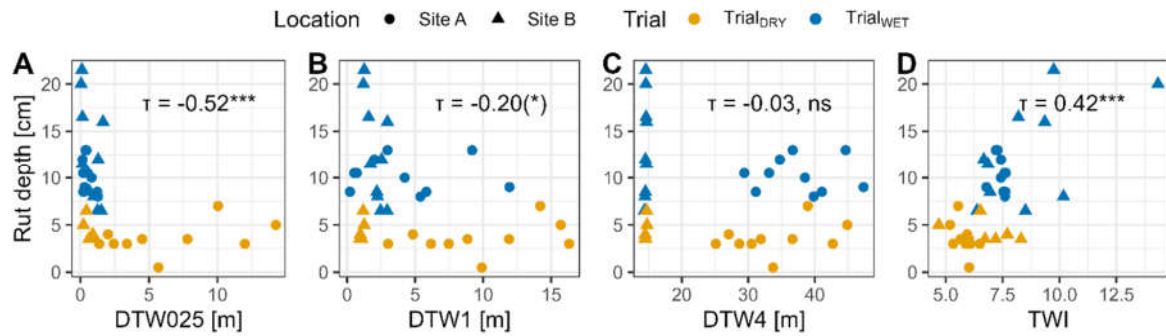


Figure B1. Rut depth (RD) was determined after four passes of a forwarder, driving on two Sites (A and B, Figure 2), during two seasons (Trial_{WET} and Trial_{DRY}, conducted under different moisture conditions). RD was compared to SWC values, determined for undisturbed soil cores (A) and SWC values predicted by a random forest model trained on manually obtained IMT measurements (B, see Figure 1) and predicted by a model trained data from a continuously measuring soil sensor network (SSN, C). Correlations were evaluated using Kendall's τ . The correlation of all values is given in black, blue and yellow show the Trials during wet and dry conditions. Significance levels are indicated by *** for $p < 0.001$, ** for 0.001-0.01, * for 0.01-0.05, (*) for 0.05-0.10, and 'ns' for $p > 0.10$.

476 **Appendix C**

477 Considering the significance of the topographic indices DTW and TWI in the development of the SWC models (Figure 4),
478 we aimed to compare RD with both indices. Notably, RD exhibited a clear correlation with DTW025, the most conservative
479 DTW scenario (Figure C1). TWI also demonstrated a correlation with RD.



480

Figure C1: Rut depth (RD) was determined after four passes of a forwarder, driving on two Sites (A and B), during two conditions (Trial_{WET} and Trial_{DRY}). RD was compared to the topographic indices depth-to-water (DTW), calculated with different flow initiation areas (0.25 – 4.00 ha), and the topographic wetness index. Correlations were evaluated using Kendall's τ and significance levels are indicated by *** for $p < 0.001$, ** for 0.001-0.01, * for 0.01-0.05, (*) for 0.05-0.10, and 'ns' for $p > 0.10$.

481 While showing significant correlations, the nature of these static maps does not allow for the representation of current moisture
482 conditions. This limitation was overcome when using the predicted (or observed) values of SWC.

483

485 **6 References**

- 486 Ågren, A., Larson, J., Paul, S. S., Laudon, H., and Lidberg, W.: Use of multiple LIDAR-derived digital terrain indices and
 487 machine learning for high-resolution national-scale soil moisture mapping of the Swedish forest landscape, *Geoderma*,
 488 404, 115280, <https://doi.org/10.1016/j.geoderma.2021.115280>, 2021.
- 489 Ågren, A., Lidberg, W., and Ring, E.: Mapping Temporal Dynamics in a Forest Stream Network—Implications for Riparian
 490 Forest Management, *Forests*, 6, 2982–3001, <https://doi.org/10.3390/f6092982>, 2015.
- 491 Ågren, A., Lidberg, W., Strömberg, M., Ogilvie, J., and Arp, P.: Evaluating digital terrain indices for soil wetness mapping –
 492 a Swedish case study, *Hydrology and Earth System Sciences*, 18, 3623–3634, <https://doi.org/10.5194/hess-18-3623-2014>,
 493 2014.
- 494 Ala-Ilomäki, J., Lindeman, H., Mola-Yudego, B., Prinz, R., Väätäinen, K., Talbot, B., and Routa, J.: The effect of bogie track
 495 and forwarder design on rut formation in a peatland, *International Journal of Forest Engineering*, 45, 1–8,
 496 <https://doi.org/10.1080/14942119.2021.1935167>, 2021.
- 497 Allman, M., Jankovský, M., Messingerová, V., and Allmanová, Z.: Soil moisture content as a predictor of soil disturbance
 498 caused by wheeled forest harvesting machines on soils of the Western Carpathians, *Journal of Forestry Research*, 28,
 499 283–289, <https://doi.org/10.1007/s11676-016-0326-y>, 2017.
- 500 Ampoorter, E., van Nevel, L., Vos, B. de, Hermy, M., and Verheyen, K.: Assessing the effects of initial soil characteristics,
 501 machine mass and traffic intensity on forest soil compaction, *Forest Ecology and Management*, 260, 1664–1676,
 502 <https://doi.org/10.1016/j.foreco.2010.08.002>, 2010.
- 503 Awaida, A. and Westervelt, J.: Geographic Resources Analysis Support System (GRASS GIS), *Geographic Resources*
 504 *Analysis Support System (GRASS GIS) Software*, USA, available at: <https://grass.osgeo.org>, 2020.
- 505 Beylich, A., Oberholzer, H.-R., Schrader, S., Höper, H., and Wilke, B.-M.: Evaluation of soil compaction effects on soil biota
 506 and soil biological processes in soils, *Soil and Tillage Research*, 109, 133–143, <https://doi.org/10.1016/j.still.2010.05.010>,
 507 2010.
- 508 Bezirksregierung Köln: Landbedeckung NRW, [https://www.bezreg-koeln.nrw.de/geobasis-nrw/produkte-und-](https://www.bezreg-koeln.nrw.de/geobasis-nrw/produkte-und-dienste/luftbild-und-satellitenbildinformationen/aktuelle-luftbild-und-3)
 509 [dienste/luftbild-und-satellitenbildinformationen/aktuelle-luftbild-und-3](https://www.bezreg-koeln.nrw.de/geobasis-nrw/produkte-und-dienste/luftbild-und-satellitenbildinformationen/aktuelle-luftbild-und-3), last access: 16 November 2023, 2023.
- 510 Bezirksregierung Köln: Digitales Geländemodell DGM1 [Digital elevation model], [https://www.bezreg-](https://www.bezreg-koeln.nrw.de/brk_internet/geobasis/hoehenmodelle/digitale_gelaendemodelle/gelaendemodell/index.html)
 511 [koeln.nrw.de/brk_internet/geobasis/hoehenmodelle/digitale_gelaendemodelle/gelaendemodell/index.html](https://www.bezreg-koeln.nrw.de/brk_internet/geobasis/hoehenmodelle/digitale_gelaendemodelle/gelaendemodell/index.html), last access: 8
 512 November 2021, 2020.
- 513 Bivand, R. S.: rgrass7: Interface Between GRASS 7 Geographical Information System and R, available at: [https://CRAN.R-](https://CRAN.R-project.org/package=rgrass7)
 514 [project.org/package=rgrass7](https://CRAN.R-project.org/package=rgrass7), 2021.
- 515 Breiman, L.: Random forests, *Machine Learning*, 45, 5–32, <https://doi.org/10.1023/A:1010933404324>, 2001.
- 516 Cambi, M., Certini, G., Neri, F., and Marchi, E.: The impact of heavy traffic on forest soils: A review, *Forest Ecology and*
 517 *Management*, 338, 124–138, <https://doi.org/10.1016/j.foreco.2014.11.022>, 2015.
- 518 Campbell, D. M.H., White, B., and Arp, P.: Modeling and mapping soil resistance to penetration and rutting using LiDAR-
 519 derived digital elevation data, *Journal of Soil and Water Conservation*, 68, 460–473,
 520 <https://doi.org/10.2489/jswc.68.6.460>, 2013.

521 Carranza, C., Nolet, C., Peziz, M., and van der Ploeg, M.: Root zone soil moisture estimation with Random Forest, *Journal of*
522 *Hydrology*, 593, 125840, <https://doi.org/10.1016/j.jhydrol.2020.125840>, 2021.

523 Cavalli, A., Francini, S., McRoberts, R. E., Falanga, V., Congedo, L., Fioravante, P. de, Maesano, M., Munafò, M., Chirici,
524 G., and Scarascia Mugnozza, G.: Estimating Afforestation Area Using Landsat Time Series and Photointerpreted
525 Datasets, *Remote Sensing*, 15, 923, <https://doi.org/10.3390/rs15040923>, 2023.

526 Chen, T., He, T., Benesty, M., Khotilovich, V., Tang, Y., Cho, H., Chen, K., Mitchell, R., Cano, I., Zhou, T., Li, M., Xie, J.,
527 Lin, M., Geng, Y., and Li, Y.: xgboost: Extreme Gradient Boosting, <https://CRAN.R-project.org/package=xgboost>, last
528 access: 9 November 2021, 2021.

529 Copernicus Climate Change Service: ERA5-Land hourly data from 2001 to present, 2019.

530 Crawford, L. J., Heinse, R., Kimsey, M. J., and Page-Dumroese, D. S.: Soil Sustainability and Harvest Operations, General
531 Technical Report RMRS, <https://doi.org/10.2737/RMRS-GTR-421>, 2021.

532 Curzon, M. T., Slesak, R. A., Palik, B. J., and Schwager, J. K.: Harvest impacts to stand development and soil properties
533 across soil textures: 25-year response of the aspen Lake States LTSP installations, *Forest Ecology and Management*, 504,
534 119809, <https://doi.org/10.1016/j.foreco.2021.119809>, 2022.

535 D'Acqui, L. P., Certini, G., Cambi, M., and Marchi, E.: Machinery's impact on forest soil porosity, *Journal of Terramechanics*,
536 91, 65–71, <https://doi.org/10.1016/j.jterra.2020.05.002>, 2020.

537 DeArmond, D., Ferraz, J., and Higuchi, N.: Natural Recovery of Skid Trails. A Review, *Canadian Journal of Forest Research*,
538 <https://doi.org/10.1139/cjfr-2020-0419>, 2021.

539 Eijkelkamp Agrisearch Equipment: User Manual for the Moisture Meter type HH2,
540 https://www.eijkelkamp.com/download.php?file=M1142602e_Soil_moisture_meter_flab.pdf, last access: 7 August
541 2020, 2013.

542 Eliasson, L.: Effects of forwarder tyre pressure on rut formation and soil compaction, *Silva Fennica*, 39, 549–557,
543 <https://doi.org/10.14214/sf.366>, available at: <http://www.metla.fi/silvafennica/full/sf39/sf394549.pdf>, 2005.

544 Finnish Meteorological Institute: Harvester Seasons,
545 https://harvesterseasons.com/HarvesterSeasons_Description2pager_v2.pdf, last access: 8 November 2023, 2023.

546 Fjeld, D., Persson, M., Fransson, J. E.S., Bjerketvedt, J., and Bråthen, M.: Modelling forest road trafficability with satellite-
547 based soil moisture variables, *International Journal of Forest Engineering*, 35, 93–104,
548 <https://doi.org/10.1080/14942119.2023.2276628>, 2024.

549 Francesca, V., Osvaldo, F., Stefano, P., and Paola, R. P.: Soil Moisture Measurements: Comparison of Instrumentation
550 Performances, *J. Irrig. Drain Eng.*, 136, 81–89, [https://doi.org/10.1061/\(ASCE\)0733-9437\(2010\)136:2\(81\)](https://doi.org/10.1061/(ASCE)0733-9437(2010)136:2(81)), 2010.

551 Grüll, M.: Den Waldboden schonen–Vorsorgender Bodenschutz beim Einsatz von Holzerntetechnik [Soil protection in forest
552 operations], *Eberswalder Forstliche Schriftenreihe*, 47, 37–44, available at:
553 [https://www.waldwissen.net/assets/technik/holzernte/boden/lfe_bodenschutz/download/lfe_bodenschutz_originalbeitrag](https://www.waldwissen.net/assets/technik/holzernte/boden/lfe_bodenschutz/download/lfe_bodenschutz_originalbeitrag.pdf)
554 [.pdf](https://www.waldwissen.net/assets/technik/holzernte/boden/lfe_bodenschutz/download/lfe_bodenschutz_originalbeitrag.pdf), 2011.

555 Guo, M., Li, J., Sheng, C., Xu, J., and Wu, L.: A Review of Wetland Remote Sensing, *Sensors (Basel, Switzerland)*, 17,
556 <https://doi.org/10.3390/s17040777>, 2017.

557 Hamner, B. and Frasco, M.: Metrics: Evaluation Metrics for Machine Learning, available at: [https://CRAN.R-](https://CRAN.R-project.org/package=Metrics)
558 [project.org/package=Metrics](https://CRAN.R-project.org/package=Metrics), 2018.

559 Hansson, L., Šimůnek, J., Ring, E., Bishop, K., and Gärdenäs, A. I.: Soil Compaction Effects on Root-Zone Hydrology and
560 Vegetation in Boreal Forest Clearcuts, *Soil Sci. Soc. Am. j.*, 83, 239, <https://doi.org/10.2136/sssaj2018.08.0302>, 2019.

561 Hauglin, M., Rahlf, J., Schumacher, J., Astrup, R., and Breidenbach, J.: Large scale mapping of forest attributes using
562 heterogeneous sets of airborne laser scanning and National Forest Inventory data, *Forest Ecosystems*, 8, 65,
563 <https://doi.org/10.1186/s40663-021-00338-4>, 2021.

564 Heppelmann, J. B., Talbot, B., Antón Fernández, C., and Astrup, R.: Depth-to-water maps as predictors of rut severity in fully
565 mechanized harvesting operations, *International Journal of Forest Engineering*, 33, 108–118,
566 <https://doi.org/10.1080/14942119.2022.2044724>, 2022.

567 Heubaum, F.: Bodenschutz im Staatsbetrieb Sachsenforst [Soil protection]: Projekte zur Technologieerprobung, Staatsbetrieb
568 Sachsenforst, https://www.sbs.sachsen.de/download/Bodenschutz_Projekte_2015_09_30.pdf, last access: 5 November
569 2021, 2015.

570 Hijmans, R. J.: raster: Geographic Data Analysis and Modeling, available at: <https://CRAN.R-project.org/package=raster>,
571 2020.

572 Hillel, D.: Environmental soil physics: Fundamentals, applications, and environmental considerations, Elsevier, San Diego,
573 California, 1998.

574 Hoffmann, S., Schönauer, M., Heppelmann, J., Asikainen, A., Cacot, E., Eberhard, B., Hasenauer, H., Ivanovs, J., Jaeger, D.,
575 Lazdins, A., Mohtashami, S., Moskalik, T., Nordfjell, T., Stereńczak, K., Talbot, B., Uusitalo, J., Vuillermoz, M., and
576 Astrup, R.: Trafficability Prediction Using Depth-to-Water Maps: the Status of Application in Northern and Central
577 European Forestry, *Curr Forestry Rep*, 338, 124, <https://doi.org/10.1007/s40725-021-00153-8>, 2022.

578 Horn, R., Vossbrink, J., Peth, S., and Becker, S.: Impact of modern forest vehicles on soil physical properties, *Forest Ecology
579 and Management*, 248, 56–63, <https://doi.org/10.1016/j.foreco.2007.02.037>, 2007.

580 James, S. E., Pärtel, M., Wilson, S. D., and Peltzer, D. A.: Temporal heterogeneity of soil moisture in grassland and forest,
581 *Journal of Ecology*, 234–239, 2003.

582 Jones, M.-F. and Arp, P.: Soil Trafficability Forecasting, *Open Journal of Forestry*, 9, 296–322,
583 <https://doi.org/10.4236/ojf.2019.94017>, 2019.

584 Jones, M.-F. and Arp, P.: Relating Cone Penetration and Rutting Resistance to Variations in Forest Soil Properties and Daily
585 Moisture Fluctuations, *Open Journal of Soil Science*, 07, 149–171, <https://doi.org/10.4236/ojss.2017.77012>, 2017.

586 Kelliher, F. M., Leuning, R., and Schulze, E. D.: Evaporation and canopy characteristics of coniferous forests and grasslands,
587 *Oecologia*, 95, 153–163, <https://doi.org/10.1007/BF00323485>, 1993.

588 Kempainen, J., Niittynen, P., Riihimäki, H., and Luoto, M.: Modelling soil moisture in a high-latitude landscape using LiDAR
589 and soil data, *Earth Surf. Process. Landforms*, 43, 1019–1031, <https://doi.org/10.1002/esp.4301>, 2018.

590 Koen Hufkens, Reto Stauffer, and Elio Campitelli: khufkens/ecmwfr: ecmwfr, Zenodo, 2019.

591 Kristensen, J. A., Balstrøm, T., Jones, R. J. A., Jones, A., Montanarella, L., Panagos, P., and Breuning-Madsen, H.:
592 Development of a harmonised soil profile analytical database for Europe: a resource for supporting regional soil
593 management, *SOIL*, 5, 289–301, <https://doi.org/10.5194/soil-5-289-2019>, 2019.

594 Kuglerová, L., Hasselquist, E. M., Richardson, J. S., Sponseller, R. A., Kreuzweiser, D. P., and Laudon, H.: Management
595 perspectives on *Aqua incognita* Connectivity and cumulative effects of small natural and artificial streams in boreal
596 forests, *Hydrological Processes*, 31, 4238–4244, <https://doi.org/10.1002/hyp.11281>, 2017.

597 Kursa, M. B. and Rudnicki, W. R.: Feature Selection with the Boruta Package, *J. Stat. Soft.*, 36,
598 <https://doi.org/10.18637/jss.v036.i11>, 2010.

599 Labelle, E. R. and Jaeger, D.: Management Implications of Using Brush Mats for Soil Protection on Machine Operating Trails
600 during Mechanized Cut-to-Length Forest Operations, *Forests*, 10, 19, <https://doi.org/10.3390/f10010019>, 2018.

601 Labelle, E. R., Poltorak, B. J., and Jaeger, D.: The role of brush mats in mitigating machine-induced soil disturbances: An
602 assessment using absolute and relative soil bulk density and penetration resistance, *Canadian Journal of Forest Research*,
603 49, 164–178, <https://doi.org/10.1139/cjfr-2018-0324>, 2019.

604 Lal, P., Singh, G., Das, N. N., Colliander, A., and Entekhabi, D.: Assessment of ERA5-Land Volumetric Soil Water Layer
605 Product Using In Situ and SMAP Soil Moisture Observations, *IEEE Geosci. Remote Sensing Lett.*, 19, 1–5,
606 <https://doi.org/10.1109/LGRS.2022.3223985>, 2022.

607 Larson, J., Lidberg, W., Ågren, A. M., and Laudon, H.: Predicting soil moisture conditions across a heterogeneous boreal
608 catchment using terrain indices, 26, 2022.

609 Leach, J. A., Lidberg, W., Kuglerová, L., Peralta-Tapia, A., Ågren, A., and Laudon, H.: Evaluating topography-based
610 predictions of shallow lateral groundwater discharge zones for a boreal lake-stream system, *Water Resources Research*,
611 53, 5420–5437, <https://doi.org/10.1002/2016WR019804>, 2017.

612 Lidberg, W., Nilsson, M., and Ågren, A.: Using machine learning to generate high-resolution wet area maps for planning
613 forest management: A study in a boreal forest landscape, *Ambio*, 49, 475–486, <https://doi.org/10.1007/s13280-019-01196-9>, 2020.

615 Mattila, U. and Tokola, T.: Terrain mobility estimation using TWI and airborne gamma-ray data, *Journal of environmental*
616 *management*, 232, 531–536, <https://doi.org/10.1016/j.jenvman.2018.11.081>, 2019.

617 McNabb, D. H., Startsev, A. D., and Nguyen, H.: Soil Wetness and Traffic Level Effects on Bulk Density and Air-Filled
618 Porosity of Compacted Boreal Forest Soils, *Soil Science Society of America Journal*, 65, 1238–1247,
619 <https://doi.org/10.2136/sssaj2001.6541238x>, 2001.

620 Mohtashami, S., Eliasson, L., Jansson, G., and Sonesson, J.: Influence of soil type, cartographic depth-to-water, road
621 reinforcement and traffic intensity on rut formation in logging operations: a survey study in Sweden, *Silva Fennica*, 51,
622 <https://doi.org/10.14214/sf.2018>, 2017.

623 Moore, I. D., Grayson, R. B., and Ladson, A. R.: Digital terrain modelling: A review of hydrological, geomorphological, and
624 biological applications, *Hydrol. Process.*, 5, 3–30, <https://doi.org/10.1002/hyp.3360050103>, 1991.

625 Muñoz-Sabater, J., Dutra, E., Agustí-Panareda, A., Albergel, C., Arduini, G., Balsamo, G., Boussetta, S., Choulga, M.,
626 Harrigan, S., Hersbach, H., Martens, B., Miralles, D. G., Piles, M., Rodríguez-Fernández, N. J., Zsoter, E., Buontempo,
627 C., and Thépaut, J.-N.: ERA5-Land: a state-of-the-art global reanalysis dataset for land applications, *Earth Syst. Sci. Data*,
628 13, 4349–4383, <https://doi.org/10.5194/essd-13-4349-2021>, 2021.

629 Murphy, P. N. C., Ogilvie, J., Meng, F.-R., White, B., Bhatti, J. S., and Arp, P.: Modelling and mapping topographic variations
630 in forest soils at high resolution: A case study, *Ecological Modelling*, 222, 2314–2332,
631 <https://doi.org/10.1016/j.ecolmodel.2011.01.003>, 2011.

632 Murphy, P. N. C., Ogilvie, J., and Arp, P.: Topographic modelling of soil moisture conditions: A comparison and verification
633 of two models, *European Journal of Soil Science*, 60, 94–109, <https://doi.org/10.1111/j.1365-2389.2008.01094.x>, 2009.

634 Murphy, P. N. C., Ogilvie, J., Connor, K., and Arp, P.: Mapping wetlands: A comparison of two different approaches for New

635 Brunswick, Canada, WETLANDS, 27, 846–854, [https://doi.org/10.1672/0277-5212\(2007\)27\[846:MWACOT\]2.0.CO;2](https://doi.org/10.1672/0277-5212(2007)27[846:MWACOT]2.0.CO;2),
636 2007.

637 Oliveira, V. A., Rodrigues, A. F., Morais, M. A. V., Terra, M. d. C. N. S., Guo, L., and Mello, C. R.: Spatiotemporal modelling
638 of soil moisture in an Atlantic forest through machine learning algorithms, *Eur J Soil Sci*, 72, 1969–1987,
639 <https://doi.org/10.1111/ejss.13123>, 2021.

640 Peng, J., Albergel, C., Balenzano, A., Brocca, L., Cartus, O., Cosh, M. H., Crow, W. T., Dabrowska-Zielinska, K., Dadson,
641 S., Davidson, M. W.J., Rosnay, P. de, Dorigo, W., Gruber, A., Hagemann, S., Hirschi, M., Kerr, Y. H., Lovergine, F.,
642 Mahecha, M. D., Marzahn, P., Mattia, F., Musial, J. P., Preuschmann, S., Reichle, R. H., Satalino, G., Silgram, M., van
643 Bodegom, P. M., Verhoest, N. E.C., Wagner, W., Walker, J. P., Wegmüller, U., and Loew, A.: A roadmap for high-
644 resolution satellite soil moisture applications – confronting product characteristics with user requirements, *Remote
645 Sensing of Environment*, 252, 112162, <https://doi.org/10.1016/j.rse.2020.112162>, 2021.

646 Picchio, R., Latterini, F., Mederski, P. S., Tocci, D., Venanzi, R., Stefanoni, W., and Pari, L.: Applications of GIS-Based
647 Software to Improve the Sustainability of a Forwarding Operation in Central Italy, *Sustainability*, 12, 5716,
648 <https://doi.org/10.3390/su12145716>, 2020.

649 Poltorak, B. J., Labelle, E. R., and Jaeger, D.: Soil displacement during ground-based mechanized forest operations using
650 mixed-wood brush mats, *Soil and Tillage Research*, 179, 96–104, <https://doi.org/10.1016/j.still.2018.02.005>, 2018.

651 Quinn, P., Beven, K., Chevallier, P., and Planchon, O.: The prediction of hillslope flow paths for distributed hydrological
652 modelling using digital terrain models, *Hydrol. Process.*, 5, 59–79, <https://doi.org/10.1002/hyp.3360050106>, 1991.

653 R Core Team: R: A Language and Environment for Statistical Computing, The R Foundation for Statistical Computing,
654 Vienna, Austria, 2023.

655 Ring, E., Ågren, A., Bergkvist, I., Finér, L., Johansson, F., and Högbom, L.: A guide to using wet area maps in forestry: En
656 guide för hur man kan använda markfuktighetskarter i skogsbruket, ARBETSRAPPORT 1051-2020, Uppsala, Sweden,
657 2022.

658 Schönauer, M. and Maack, J.: R-code for calculating depth-to-water (DTW) maps using GRASS GIS (Version v1), Zenodo,
659 <https://doi.org/10.5281/zenodo.5638518>, 2021.

660 Schönauer, M., Prinz, R., Väättäinen, K., Astrup, R., Pszenny, D., Lindeman, H., and Jaeger, D.: Spatio-temporal prediction
661 of soil moisture using soil maps, topographic indices and SMAP retrievals, *International Journal of Applied Earth
662 Observation and Geoinformation*, 108, 102730, <https://doi.org/10.1016/j.jag.2022.102730>, 2022.

663 Schönauer, M., Hoffmann, S., Maack, J., Jansen, M., and Jaeger, D.: Comparison of Selected Terramechanical Test
664 Procedures and Cartographic Indices to Predict Rutting Caused by Machine Traffic during a Cut-to-Length Thinning
665 Operation, *Forests*, 12, 113, <https://doi.org/10.3390/f12020113>, 2021a.

666 Schönauer, M., Väättäinen, K., Prinz, R., Lindeman, H., Pszenny, D., Jansen, M., Maack, J., Talbot, B., Astrup, R., and Jaeger,
667 D.: Spatio-temporal prediction of soil moisture and soil strength by depth-to-water maps, *International Journal of Applied
668 Earth Observation and Geoinformation*, 105, 102614, <https://doi.org/10.1016/j.jag.2021.102614>, available at:
669 <https://www.sciencedirect.com/science/article/pii/S0303243421003214>, 2021b.

670 Sirén, M., Salmivaara, A., Ala-Ilomäki, J., Launiainen, S., Lindeman, H., Uusitalo, J., Sutinen, R., and Hänninen, P.:
671 Predicting forwarder rut formation on fine-grained mineral soils, *Scandinavian Journal of Forest Research*, 34, 145–154,
672 <https://doi.org/10.1080/02827581.2018.1562567>, 2019.

673 Sørensen, R. and Seibert, J.: Effects of DEM resolution on the calculation of topographical indices: TWI and its components,
674 *Journal of Hydrology*, 347, 79–89, <https://doi.org/10.1016/j.jhydrol.2007.09.001>, 2007.

675 Suvinen, A. and Saarilahti, M.: Measuring the mobility parameters of forwarders using GPS and CAN bus techniques, *Journal*
676 *of Terramechanics*, 43, 237–252, <https://doi.org/10.1016/j.jterra.2005.12.005>, 2006.

677 Tromp-van Meerveld, H. J. and McDonnell, J. J.: On the interrelations between topography, soil depth, soil moisture,
678 transpiration rates and species distribution at the hillslope scale, *Advances in Water Resources*, 29, 293–310,
679 <https://doi.org/10.1016/j.advwatres.2005.02.016>, 2006.

680 Uusitalo, J., Ala-Ilomäki, J., Lindeman, H., Toivio, J., and Sirén, M.: Predicting rut depth induced by an 8-wheeled forwarder
681 in fine-grained boreal forest soils, *Annals of forest science*, 77, <https://doi.org/10.1007/s13595-020-00948-y>, 2020.

682 Uusitalo, J., Ala-Ilomäki, J., Lindeman, H., Toivio, J., and Sirén, M.: Modelling soil moisture – soil strength relationship of
683 fine-grained upland forest soils, *Silva Fennica*, 53, <https://doi.org/10.14214/sf.10050>, 2019.

684 Vega-Nieva, D. J., Murphy, P. N. C., Castonguay, M., Ogilvie, J., and Arp, P.: A modular terrain model for daily variations
685 in machine-specific forest soil trafficability, *Canadian Journal of Soil Science*, 89, 93–109,
686 <https://doi.org/10.4141/CJSS06033>, 2009.

687 Walker, J. P., Willgoose, G. R., and Kalma, J. D.: In situ measurement of soil moisture: a comparison of techniques, *Journal*
688 *of Hydrology*, 293, 85–99, <https://doi.org/10.1016/j.jhydrol.2004.01.008>, 2004.

689 White, B., Ogilvie, J., Campbell, D. M.H., Hiltz, D., Gauthier, B., Chisholm, H. K., Wen, H. K., Murphy, P. N. C., and Arp,
690 P.: Using the Cartographic Depth-to-Water Index to Locate Small Streams and Associated Wet Areas across Landscapes,
691 *Canadian Water Resources Journal*, 37, 333–347, <https://doi.org/10.4296/cwrj2011-909>, 2012.

692 Wright, M. N. and Ziegler, A.: ranger: A Fast Implementation of Random Forests for High Dimensional Data in C++ and R,
693 *J. Stat. Soft.*, 77, <https://doi.org/10.18637/jss.v077.i01>, 2017.

694